

Forbidden coherent transfer observed between two realizations of quasi-harmonic spin systems

S. Bertaina,^{1,*} G. Yue,² C-E Dutoit,¹ and I. Chiorescu²

¹*Aix-Marseille Université, CNRS, IM2NP (UMR 7334), Marseille, France*

²*Department of Physics and The National High Magnetic Field Laboratory, Florida State University, Tallahassee, Florida 32310, USA*

(Dated: December 14, 2024)

The multi-level system $^{55}\text{Mn}^{2+}$ is used to generate two pseudo-harmonic level systems, as representations of the same electronic sextuplet at different nuclear spin projections. The systems are coupled using a forbidden nuclear transition induced by the crystalline anisotropy. We demonstrate Rabi oscillations between the two representations in conditions similar to two coupled quasi-harmonic quantum oscillators. Rabi oscillations are performed at a detuned pumping frequency which matches energy difference between electro-nuclear states of different oscillators. We measure a coupling stronger than the decoherence rate, to indicate the possibility fast information exchange between the systems.

PACS numbers: 03.67.-a 71.70.Ch 75.10.Dg 76.30Da

I. INTRODUCTION

Recent advances in single spin measurements in gated nanostructures¹ and quantum dots² show that spin-based materials have impact in quantum technologies. One example is constituted by multi-level spin systems which have well defined spin Hamiltonians, sufficiently large to be used as multi-qubit implementations³ and small enough to be studied by exact numerical methods. When diluted in non-magnetic matrices, electronic spins attain large coherence times⁴⁻⁶ and present the possibility to be coupled coherently to nuclear spins. In such implementations, magnetic ions (such as rare-earth elements) play an essential role^{7,8} with demonstrated capability to coherently exchange information between electron spins and nuclei^{9,10} as well as optical photons¹¹. In the current work, we are focusing on a $3d$ element, Mn, which has a very low anisotropy and thus less stringent conditions for the orientation of the external field. This offers more flexibility for on-chip applications and towards the use of long-lived nuclear spin states for storage and retrieval of quantum information. We analyze the feasibility of combining high spin electronic and nuclear systems to demonstrate coherent exchange of information between electro-nuclear states. To that end, we make use of the so-called forbidden transitions.

$^{55}\text{Mn}^{+2}$ ions diluted in a MgO matrix show electron spin resonance (ESR) transitions with $\Delta S_z = 1$ and $\Delta m_I = 0$ (S_z and m_I are projections of the electronic and nuclear $S = I = 5/2$ moments respectively) at fields separated by the hyperfine interaction in $2I + 1$ well-defined groups. However, off-diagonal couplings in the spin Hamiltonian, such as anisotropy and transverse fields terms, can activate forbidden transitions $\Delta m_I \neq 0$ and/or $\Delta S_z \neq 1$. Such transitions are essential to make the entire Hilbert space available for quantum information manipulation and can be achieved by means of non-linear multi-photon activation^{12,13}. Large Δm_I electro-

nuclear mixture can be achieved by making use of crystal and transverse fields¹⁴ as well.

The forbidden transitions reflect a coupling between different representations of the same multi- S_z system as detailed below. Although the transfer probability between electro-nuclear states is low, the coherence properties are robust and in addition it allows maneuvering the Hamiltonian in and out of the forbidden (coupled) region. We present theoretical and experimental evidence of Rabi oscillations and of a driven strong coupling regime between states belonging to such different representations. The Rabi oscillations in this multi-level system are measured using a two-tone technique we have recently developed¹⁵. In fixed static field, a first ESR pulse excites the system at any frequency detuning and a second pulse reads the difference in level population at the main resonance. As explained below, this method allows us to detune two representations of multi-level systems until they are brought in resonance, to demonstrate the strong coupling regime and a coherent transfer of information between the two systems.

II. RABI OSCILLATIONS OF THE ELECTRO-NUCLEAR TRANSITION.

The electro-nuclear Hamiltonian¹² of the Mn ions is:

$$H = H_{CF} + \gamma \vec{H}_0 \cdot \vec{S} - A \vec{S} \cdot \vec{I} + \gamma \vec{h}_{mw} \cdot \vec{S} \cos(2\pi ft) \quad (1)$$

where $\gamma = g\mu_B/h$ is the gyromagnetic ratio ($g = 2.0014$ the g -factor, μ_B Bohr's magneton and h Planck's constant), $S_{x,y,z}$ are the spin projection operators, \vec{S} is the total spin, $A = 244$ MHz is the hyperfine constant, h_{mw} and f represent the microwave amplitude and frequency respectively, and \vec{H}_0 is the static field ($\vec{H}_0 \perp \vec{h}_{mw}$). $H_{CF} = a/6[S_x^4 + S_y^4 + S_z^4]$ with $a = 55.7$ MHz the anisotropy constant, represents the crystal field anisotropy which generates a small anharmonic-

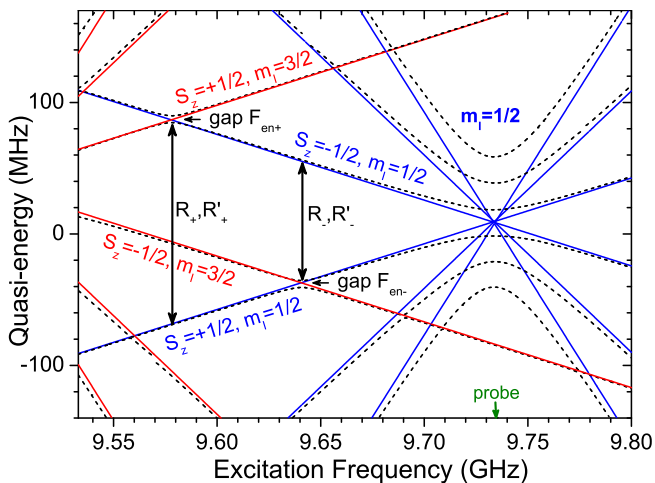


FIG. 1. (color online) Eigen-states of H in RFA approximation for low (lines) and high (dashed lines) microwave power for two sextuplets S_z : $m_I = 1/2$ (blue, right) and $3/2$ (red, left). The static field corresponds to the resonance frequency (shown by the green arrow) where the equally spaced levels collapse (for $\hbar \rightarrow 0$). Detuned Rabi oscillations, *e.g.* R_{\pm} with location shown by the double-headed arrows, can be measured for any frequency in this range.

ity of the otherwise equally spaced Zeeman levels $S_z = -5/2 \dots 5/2$.

The model describing the multiphoton Rabi oscillations observed in MgO:Mn_2^+ was reported in Ref. [12]. However, the electron-nuclear forbidden transitions were dropped off the model since their probability are weak compared to the multiphoton electronic transitions. In this work, we adapt the model to take advantage of the full Hamiltonian $S \otimes I$ whose dimensionality becomes 36. The ESR of forbidden transitions in MgO:Mn_2^+ were discussed in Refs. [16] and [17]. Here we use the rotating frame approximation (RFA) to describe the quantum dynamics of the forbidden transitions.

Previous work¹² shows that at exactly the ‘‘compensation angle’’ $\theta = \theta_c$ between \vec{H}_0 and the crystal axis z , the anharmonic effect of the H_{CF} term is compensated for and the S_z levels are equidistant. In the present study, we chose to work at the compensation angle to reduce the level structure to simple pseudo-harmonic systems and put in evidence their coupling. Note that the applied static field ensures a Zeeman splitting of $\gamma H_0 \approx f \sim 10$ GHz, much stronger than all other interactions of Eq.(1), effectively making \vec{H}_0 the quantization axis.

Exact diagonalization of Hamiltonian (1) is performed after a transformation into a frame rotating with frequency f as detailed in Ref. [12]. Coherent motion of spin projection S_z is analyzed using time-dependent Schrödinger equation and its FFT can reveal multiple Rabi frequencies and beatings (see below). In the RFA approximation, the resonance is shown in Fig. 1 by the probe arrow where all eigen-states collapse (for

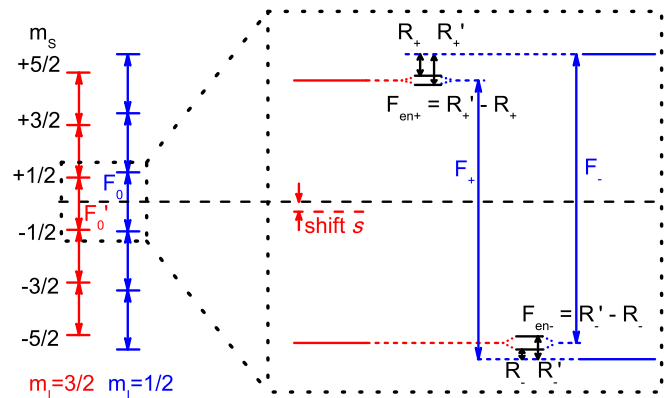


FIG. 2. (color online) Sketch of H eigen-states for $m_I = 1/2$ and $3/2$. The central four states are magnified, showing the relationships $F_0 = F_- + R_- = F_+ + R_+ = F'_0 + A$, as well as the Rabi splittings $F_{en\pm}$. The shift s (see text) enforces $R_+ \neq R_-$ and thus distinct double-headed arrows in Fig. 1.

$m_I = 1/2$, the blue sextuplet). The two sextuplets are two pseudo-harmonic oscillators as different realizations of the same set $|S_z\rangle$. The dashed lines indicate the effect of a large h_{mw} on the numerically computed dressed states.

III. EXPERIMENTAL PROCEDURE

Measurements were performed using a conventional Bruker Elexsys 680 pulse spectrometer. The second frequency source is provided by the ELDOR bridge of the spectrometer. The experiments are performed in a static field corresponding to $F_0 = 9.734$ GHz, $F_- = 9.641$ GHz and $F_+ = 9.586$ GHz. A first microwave pump pulse of frequency $f = F_{\pm}$ drives Rabi oscillations of the Mn spins. After a time longer than the Rabi decay time but much shorter than the relaxation time, a second ($\pi/2$) pulse at $f = F_0$ probes the S_z component, using the intensity of the Free Induction Decay (FID) signal (see Ref. 15 for a detailed explanation).

For clarity, only the case of $m_I = 3/2$ and $1/2$ is presented here. The sextuplets are sketched in Fig. 2 together with a magnified representation of the main ESR transition, between states $S_z = \pm 1/2$. The Zeeman splittings are $F_0 = f$ and $F'_0 = F_0 - A$ for $m_I = 1/2$ and $3/2$ respectively. The two transitions are shifted by an amount s which is evaluated by Drumheller¹⁸ as a second order perturbation in A and generates the vertical shift between sextuplets in Fig. 1. The shift $s \approx 33$ MHz is in good agreement with the theoretical estimation¹⁸ of ~ 44 MHz. Consequently, forbidden couplings between sextuplets occur at different frequencies $F_{\pm} = F_0 - A/2 \mp s$, allowing their individual excitation by an adequate detuning of the drive frequency f . The frequency of Rabi oscillations is shown by double headed arrows $R_{\pm} = F_0 - F_{\pm} = A/2 \pm s$. Moreover, if the electro-nuclear coupling between the two sextuplets is larger than the decoherence rate, a splitting of the Rabi

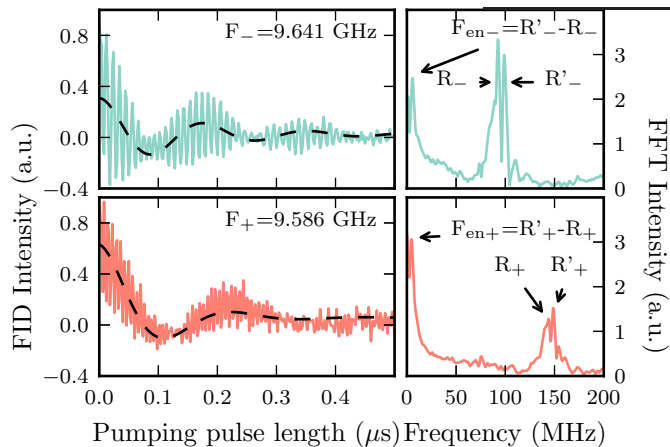


FIG. 3. (color online) Rabi oscillations (left panel) for drive frequencies F_{\pm} matching forbidden resonance conditions between two pseudo-harmonic level systems (see Fig. 2). The dashed line is a beating between two Rabi frequencies, demonstrating a coupling between the two systems stronger than the Rabi decay time. Corresponding FFT spectra are shown in the right panel, with visible strong coupling splittings $F_{en\pm} = R'_{\pm} - R_{\pm}$.

frequencies should be observed ($F_{en\pm} = R'_{\pm} - R_{\pm}$) as illustrated in Fig. 2 and numerically calculated in Fig. 1.

IV. RESULTS AND DISCUSSIONS

Experimental results are presented in Fig. 3 as time-domain Rabi oscillations (left panel) and their Fast Fourier Transform (FFT) spectra (right panel). One observes that the Rabi frequencies are remarkably large for a spin system, with $R_- \approx 100$ MHz and $R_+ \approx 150$ MHz, comparable to Rabi rates achieved in quantum dots¹⁹. Also, the coupling between the two electronic systems is sufficiently strong to overpass the Rabi decay rate of ~ 250 ns. This leads to normal mode splitting of the two Rabi frequencies by an amount $F_{en\pm} = R'_{\pm} - R_{\pm} = 4.5$ MHz and 5.7 MHz, respectively. In the left panel of Fig. 3, the dashed line shows the F_{en+} and F_{en-} beatings with a damping of ~ 200 ns and ~ 250 ns respectively.

The two-tone technique allows the study of coupled Rabi oscillations for any detuning, in the vicinity of F_{\pm} . FFT spectra at constant microwave power ($h_{mw} \sim 10$ G at resonance, same as in Fig. 3) are shown in Fig. 4, as a function of drive frequency around the resonances F_+ (a) and F_- (b). The symbols represent the values of R_{\pm} , R'_{\pm} (triangles) and F_{en} (circles) as FFT peaks of measured Rabi dynamics while the contour plot is calculated by exact diagonalization of H in the rotating frame. One notes how the Rabi oscillation accelerates with the detuning to large values, close to 200 MHz. The low frequency beating F_{en} is equal to the splitting of the two Rabi frequencies, when the resonance condition described

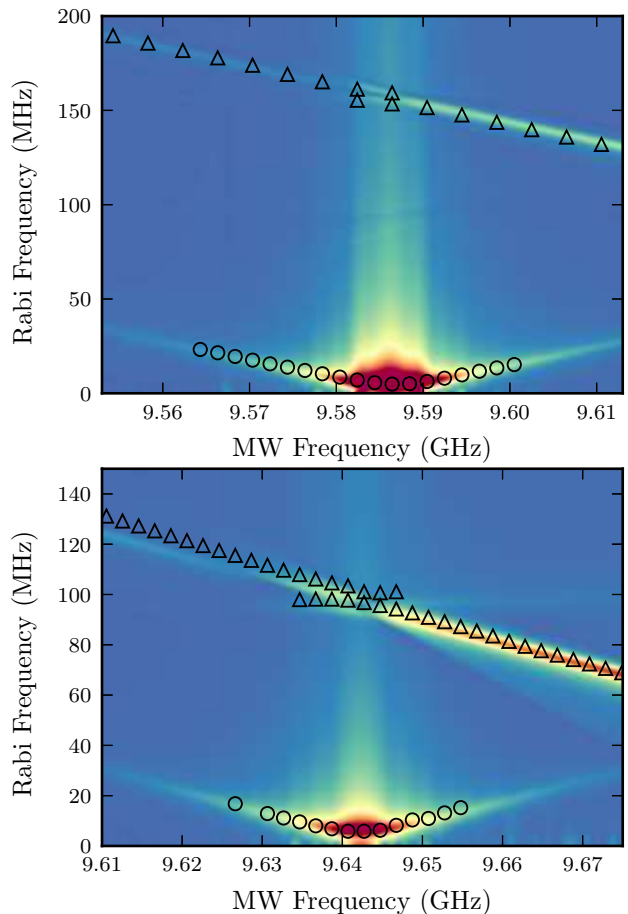


FIG. 4. (color online) FFT spectra as a function of drive frequency around F_+ (top) and F_- (bottom). The peaks location, intensity and width indicate Rabi oscillations frequency, amplitude and decay rate. The symbols are FFT peaks of measured Rabi oscillations: Δ / \circ correspond to the high / low frequency Rabi oscillations shown in Fig. 3

above (Figs. 1,2) is met. Moreover, one observes an increase of the beat frequency due to detuning, similar to the coherent motion of a two-level system (TLS) driven out of resonance. Here, $F_{en\pm}$ represent the coherent motion between two pseudo-harmonic oscillators.

The height of a FFT peak in Fig. 4 represents the amplitude of the corresponding Rabi oscillation. They are extracted and shown in Fig. 5 as a function of detuning away from F_0 . While Rabi frequency increase with detuning, the oscillation's amplitude decreases. For a TLS, the amplitude P of the Rabi frequency $F_R(\delta)$ as a function of detuning δ is described by the well-known relation²⁰:

$$P = a_1 \frac{F_R(0)^2}{F_R(0)^2 + \delta^2} + a_0 \quad (2)$$

with $a_{i=0,1} = i$ in the Rabi model while here they are fit parameters. Eq. 2 fits very well $F_{en\pm}$ data (dashed

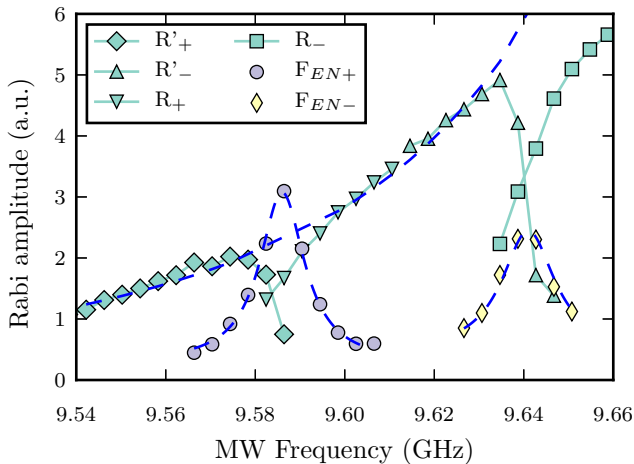


FIG. 5. (color online) Amplitudes of Rabi oscillations (FFT peak intensities from Fig. 4) as a function of drive frequency, fitted by a TLS model (2) (dotted and dashed lines). In the strong coupling region, $F_{en\pm}$ are very well described by the fit.

curves). It also describes the R_{\pm} and R'_{\pm} data (dotted curve) in regions where the dynamics \hat{R}_{\pm} is not affected by the strong coupling of the two level systems. In the coupled region $f \sim F_{\pm}$, the fit half-width at half-maximum gives very good estimations of the beat frequencies: $F_{en+} = 6.06$ MHz and $F_{en-} = 7.2$ MHz. The other fit parameters are $a_1 = 2.8$ and $2, a_0 = 0.27$ and 0.44 , for F_+ and F_- respectively.

The nature and magnitude of the forbidden transition probabilities have been studied theoretically in this system¹⁷ and they follow (here $\theta = \theta_c = 31^\circ$):

$$F_{en\pm} \propto 5 \sin 4\theta (ah_{mw}/f) [I(I+1) - m_I(m_I - 1)]. \quad (3)$$

Thus, the small anisotropy a is the essential ingredient to the coupling between the two oscillators, by enabling forbidden electronic transitions with $\Delta S_z = \Delta m_I = 1$. Notable is the dependence of $F_{en\pm}$ on microwave field h_{mw} which allows *in-situ* control over the strength of coupling between the two pseudo-harmonic oscillators. Since the TLS model (2) applies well to the forbidden transitions, the dynamics shown in Fig. 2 can now be

described by an effective 4×4 RFA Hamiltonian:

$$H_{RF} = \Delta s_z - A s_z i_z - s i_z + 2F_{en} s_x i_x + \gamma h_{mw} s_x \quad (4)$$

where $F_{en} = F_{en\pm}$, $s_{x,z}$ and $i_{x,z}$ are the Pauli matrices for the electronic and nuclear spin operator in this effective representation and $\Delta = f - (F_0 - A/2)$ is the detuning of the pump pulse by respect to $F_0 - A/2$. The coupled oscillations take place at $\Delta, A, s, F_{en} \gg \gamma h_{mw}$ in which case analytical diagonalization of H_{RF} for $h_{mw} \sim 0$ leads to two pairs of levels $S_{\pm}^{(1)} = A/4 \pm \frac{1}{2} \sqrt{(\Delta + s)^2 + F_{en}^2}$ and $S_{\pm}^{(2)} = -A/4 \pm \frac{1}{2} \sqrt{(\Delta - s)^2 + F_{en}^2}$ with F_{en} given by Eq. 3. The splitting of each pair at $\Delta = \pm s$ is F_{en} , as expected. Different from the strong coupling regime in cavity QED experiments²¹⁻²³ is the fact that here the Vacuum Rabi Splitting is observed under a sufficiently strong drive, since $F_{en\pm} \propto h_{mw}$. Resonant photons of energy hF_- (or hF_+) match the difference between $|0, e\rangle$ and $|1, g\rangle$, where 0 and 1 label the state of the pseudo-harmonic electronic spin system (operator s_z) and e, g label the nuclear state (operator i_z).

Following Eq. 3, the couplings $F_{en\pm}$ should be equal while in our experiment they are slightly different. This is due to the cavity resonance profile, centered around $\sim F_0$ and detuned at F_{\pm} with $F_+ < F_- < F_0$. Consequently, the microwave fields at F_{\pm} follow $h_{mw+} < h_{mw-}$ which leads to $F_{en+} < F_{en-}$. This case can be described by Hamiltonian (4) by replacing the term $2F_{en} s_x i_x$ with $F_{en-}(s_+ i_- + s_- i_+)/2 + F_{en+}(s_+ i_+ + s_- i_-)/2$.

In conclusion, we show coherent transfer of state population between two equidistant level systems, $|S_z, m_I = 1/2\rangle$ and $|S_z, m_I = 3/2\rangle$ by using forbidden nuclear transitions with $\Delta m_I = 1$. The coupling between systems is tunable and is stronger than the decay rate, leading to an observable splitting of the Rabi mode and a state transfer faster than the decay time. The results open the way of combining the electronic and long-lived nuclear degrees of freedom in this multi-level system.

This work was supported by NSF Grant No. DMR-1206267, CNRS-PICS CoDyLow and CNRS's research federation RENARD (FR3443) for EPR facilities. The NHMFL is supported by Cooperative Agreement Grant No. DMR-1157490 and the state of Florida.

* sylvain.bertaina@im2np.fr

¹ J. T. Muhonen, J. P. Dehollain, A. Laucht, F. E. Hudson, R. Kalra, T. Sekiguchi, K. M. Itoh, D. N. Jamieson, J. C. McCallum, A. S. Dzurak, and A. Morello, Nat. Nanotechnol. **9**, 986 (2014).

² M. Goryca, M. Koperski, P. Wojnar, T. Smoleński, T. Kazimierczuk, A. Golnik, and P. Kossacki, Phys. Rev. Lett. **113**, 227202 (2014).

³ M. N. Leuenberger and D. Loss, Nature **410**, 789 (2001).

⁴ S. Nellutla, K. Y. Choi, M. Pati, J. van Tol, I. Chiorescu,

and N. S. Dalal, Phys. Rev. Lett. **99**, (2007).

⁵ S. Bertaina, S. Gambarelli, A. Tkachuk, I. N. Kurkin, B. Malkin, A. Stepanov, and B. Barbara, Nat. Nanotechnol. **2**, 39 (2007).

⁶ S. Bertaina, S. Gambarelli, T. Mitra, B. Tsukerblat, A. Müller, and B. Barbara, Nature **453**, 203 (2008).

⁷ S. Probst, H. Rotzinger, A. V. Ustinov, and P. A. Bushev, Phys. Rev. B **92** (2015).

⁸ S. Bertaina, J. H. Shim, S. Gambarelli, B. Z. Malkin, and B. Barbara, Phys. Rev. Lett. **103**, 226402 (2009).

- ⁹ M. V. G. Dutt, L. Childress, L. Jiang, E. Togan, J. Maze, F. Jelezko, A. S. Zibrov, P. R. Hemmer, and M. D. Lukin, *Science* **316**, 1312 (2007).
- ¹⁰ G. Wolfowicz, H. Maier-Flaig, R. Marino, A. Ferrier, H. Vezin, J. J. L. Morton, and P. Goldner, *Phys. Rev. Lett.* **114**, 170503 (2015).
- ¹¹ C. Clausen, I. Usmani, F. Bussières, N. Sangouard, M. Afzelius, H. de Riedmatten, and N. Gisin, *Nature* **469**, 508 (2011).
- ¹² S. Bertaina, L. Chen, N. Groll, J. Van Tol, N. S. Dalal, and I. Chiorescu, *Phys. Rev. Lett.* **102**, 50501 (2009).
- ¹³ S. Bertaina, N. Groll, L. Chen, and I. Chiorescu, *Phys. Rev. B* **84**, 134433 (2011).
- ¹⁴ M. S. Fataftah, J. M. Zadrozny, S. C. Coste, M. J. Graham, D. M. Rogers, and D. E. Freedman, *J. Am. Chem. Soc.* **138**, 1344 (2016).
- ¹⁵ S. Bertaina, M. Martens, M. Egels, D. Barakel, and I. Chiorescu, *Phys. Rev. B* **92**, 24408 (2015).
- ¹⁶ G. Wolga and R. Tseng, *Phys. Rev.* **133**, A1563 (1964).
- ¹⁷ S. R. P. Smith, P. V. Auzins, and J. E. Wertz, *Phys. Rev.* **166**, 222 (1968).
- ¹⁸ J. E. Drumheller and R. S. Rubins, *Phys. Rev.* **133**, A1099 (1964).
- ¹⁹ J. Yoneda, T. Otsuka, T. Nakajima, T. Takakura, T. Obata, M. Pioro-Ladrière, H. Lu, C. J. Palmstrøm, A. C. Gossard, and S. Tarucha, *Phys. Rev. Lett.* **113**, 267601 (2014).
- ²⁰ C. Cohen-Tannoudji, B. Diu, and F. Laloë, *Quantum Mechanics Vol.2* (John Wiley & Sons, Inc., New York, 2006) p. vol 2.
- ²¹ I. Chiorescu, N. Groll, S. Bertaina, T. Mori, and S. Miyashita, *Phys. Rev. B* **82**, 24413 (2010).
- ²² Y. Kubo, F. R. Ong, P. Bertet, D. Vion, V. Jacques, D. Zheng, A. Dreau, J. F. Roch, A. Auffeves, F. Jelezko, J. Wrachtrup, M. F. Barthe, P. Bergonzo, and D. Esteve, *Phys. Rev. Lett.* **105** (2010).
- ²³ D. I. Schuster, A. P. Sears, E. Ginossar, L. DiCarlo, L. Frunzio, J. J. L. Morton, H. Wu, G. A. D. Briggs, B. B. Buckley, D. D. Awschalom, and R. J. Schoelkopf, *Phys. Rev. Lett.* **105** (2010).